The Order-Disorder Transition in Cu_2ZnSnS_4 – A Neutron Scattering Investigation

A. Ritscher[1,2], M. Hoelzel[3], M. Lerch[*] [1]

[1] *Institut für Chemie, Technische Universität Berlin, Straße des 17.Juni 135, 10623 Berlin, Germany*

[2] *Helmholtz-Zentrum Berlin für Materialien und Energie, Hahn-Meitner-Platz 1, 14109 Berlin, Germany*

[3] *Heinz Maier-Leibnitz Zentrum (MLZ), Technische Universität München, Lichtenbergstr.1, 85748 Garching, Germany*

[*] corresponding author: *martin.lerch@tu-berlin.de*

Keywords: CZTS powder, mechanochemical synthesis, neutron scattering, cation distribution, Rietveld refinement, order-disorder transition

Abstract

In this work a series of stoichiometric Cu_2ZnSnS_4 (CZTS) samples annealed at different temperatures in the range of 473 – 623 K were investigated. The temperature dependence of the Cu/Zn-order-disorder behavior was analyzed by neutron powder diffraction measurements. Cu fully occupies the 2a and Sn the 2b position within the whole temperature range. For Zn and the remaining Cu on sites 2d and 2c, a clear change from ordered to disordered kesterite structure is found. The critical temperature T_c for this Landau-type second order transition was determined as 552 ± 2 K. It was found that in Cu_2ZnSnS_4 very long annealing times are necessary to reach equilibrium at low temperatures.

1 Introduction

The quaternary chalcogenide Cu_2ZnSnS_4 and related compounds recently attract much attention as prospective absorber materials for thin film solar cell technology. This direct band gap p-type semiconductor with an optical band gap energy value of 1.5 eV and an absorption coefficient in the order of 10^{-4} cm^{-1} contains only abundant and non-toxic elements [1-3]. Consequently, it would be a suitable alternative to other chalcogenide-based absorber materials such as CdTe or CIGS ($CuIn_xGa_{(1-x)}Se_2$) that are currently used. Up to now record efficiencies of CZTS-based thin films of 12.6 % are reported for devices that additionally contain selenium [4]. Yet, compared to the currently used chalcopyrite materials, efficiencies are significantly lower due to the limiting open-circuit voltage V_{oc}. It is assumed that the low V_{oc} is caused by the existence of band gap fluctuations. Various reasons for the decrease of the effective band gap such as inclusions of stannite or the occurrence of $\left[Cu_{Zn}^{-} + Sn_{Zn}^{2+}\right]$ defect complexes were suggested [3, 5]. Recently it was shown by experimental and theoretical studies that the band gap fluctuations of 100 – 200 meV can be primary attributed to the disorder

among the Cu and Zn cations in the crystal structure [6]. The significant reduction of the effective band gap is caused by the high number of [Cu_{Zn} + Zn_{Cu}] defect pairs and the clustering of those defect pairs was studied by *ab initio* calculations [6].

Cu_2ZnSnS_4 crystallizes in the kesterite type (space group $I\bar{4}$) [7, 8]. Four different cation sites are available in the structure. In the fully ordered kesterite structure Sn is located on site 2*b* (0, 0, ½), one Cu occupies the 2*a* (0, 0, 0) position, the remaining Cu is located on position 2*c* (0, ½, ¼), Zn on 2*d* (0, ½, ¾). The sphalerite-type derived crystal structure can be described by the stacking of cation layers along the c-axis (Cu/Sn on z = 0 and z = 1/2; Cu/Zn at z = 1/4 and z = 3/4) separated by layers of sulfur atoms. Diffraction studies of CZTS powder samples report a partial [9, 10] or complete disorder [11] of Cu and Zn on the 2c and 2d positions. Kesterite-type phases exhibiting a statistical distribution of Cu and Zn on the two latter sites can be described in space group $I\bar{4}2m$ with Zn and Cu occupying the 4d (0, 1/2, 1/4) Wyckoff position which is called disordered kesterite [12]. Consequently, the cation layers at z = 1/4 and z = 3/4 are involved in the order-disorder process. Furthermore, it was shown by *ab initio* calculations [13, 14] that the point defects Cu_{Zn} and Zn_{Cu} have very low formation energies and thus Cu/Zn disorder is highly possible. In Figure 1 the fully ordered and the disordered kesterite structure are depicted.

Until now only few studies on the ordering in CZTS were carried out. The local structure of defects in Cu-poor/Zn-rich material was investigated by solid-state NMR and Raman spectroscopy [15]. X-ray resonant diffraction measurements at the Cu-Kα and Zn-Kα absorption edge were carried out to analyse the Cu/Zn ordering in a CZTS single crystal [16]. Furthermore, CZTS thin films were studied to track the Cu/Zn disorder [6, 17]. In those studies near-order resonant Raman measurements of Zn rich thin films were carried out. The critical temperature for the transition from ordered to disordered kesterite was determined as 533 ± 10 K. In high temperature X-ray diffraction measurements of a kesterite powder sample using synchrotron radiation a kink in the temperature dependent lattice parameter variation is observed at 513 K [18].

For a reliable structural characterization, which is essential for tracking the decrease in the cation order, diffraction methods are preferable.

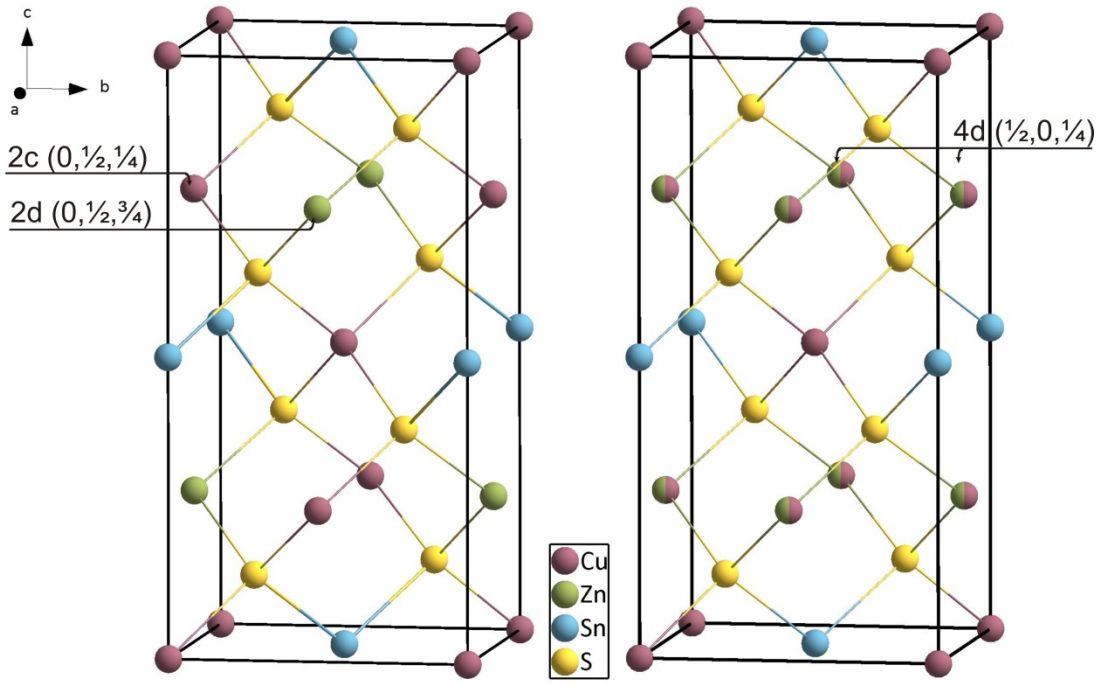

Figure 1 Unit cells of ordered (left) and disordered kesterite (right); sites involved in the order-disorder transition are labeled. In the ordered kesterite Cu occupies position 2c whereas Zn is located on 2d. In disordered kesterite the cations are statistically distributed on these two cation positions leading to a change in the space group from $I\bar{4}$ to $I\bar{4}\boldsymbol{2m}$ and consequently a change to Wyckoff position 4d.

Our recent neutron diffraction study of a powder sample cooled down from 773 K predicts that Cu fully occupies the 2a position. Zn and the remaining Cu reveal a partial disorder of the cations on the two positions 2c and 2d (approx.: 2c: 72 % Cu 28 % Zn, 2d: 28 % Cu 72 % Zn) [10].

The present work was undertaken to verify the recent results of Scragg et al. [6] and to follow the order-disorder transition in the cationic network of CZTS powder samples by diffraction techniques. Using conventional X-ray diffraction methods, Cu^{+} and Zn^{2+} are not distinguishable due to their isoelectronic character. However, those two cations show a significant difference in their neutron scattering length (b_{Cu} = 7.718(4) fm, b_{Zn} = 5.680(5) fm). Consequently, neutron diffraction is the method of choice. Ten stoichiometric CZTS powder samples were synthesized via our recently developed mechanochemical process [10]. Taking into account the recent work of Scragg et al. [17] it is clear that the time to reach equilibrium is up to more than 24 h, making *in situ*-neutron scattering measurements not useful. Consequently, various samples were prepared by quenching.

2 Experimental

2.1 Synthesis

Recently we developed a new route for an easy and fast synthesis of phase-pure and stoichiometric CZTS powders [10] where the quaternary sulfide was prepared by mechanical milling in a high energy planetary ball mill starting from the corresponding binary sulfides CuS, ZnS, and SnS followed by an

annealing step in H_2S atmosphere. In this work ten CZTS powder samples were finally annealed in sealed and evacuated silica ampoules at different temperatures in order to follow the order-disorder transition.

For each sample the binary sulfides CuS, ZnS and SnS were mixed in an atomic ratio of 2:1:1. As described in detail elsewhere [10] the starting compounds were prepared either by precipitation (CuS), sulfidation of the oxide (ZnS) or solid state reaction of the elements (SnS). The mixture was filled into an 80 ml agate grinding bowl with five 20 mm grinding balls under Ar atmosphere in a glove box. Milling was performed in a Fritsch Planetary Mono Mill PULVERISETTE 6 using a rotational speed of 350 rpm and a milling time of 5 h. The result of the mechanochemical treatment was a poorly crystalline powder.

In a second step each sample was annealed in a conventional tube furnace equipped with a SiO_2-tube under flowing reaction gas (H_2S) for 3 h at 773 K. Using inert gas (N_2 or Ar) instead of H_2S, the formation of secondary phases is observed. After reaction the sample was cooled down with a cooling rate of 60 K/h. The results of this annealing step are CZTS powders with good crystallinity.

In order to obtain powders with different order parameter, a final annealing step at different temperatures in the range of 473 – 623 K was performed. The exact heating temperatures (including sample names) were T = 473 (N1, N10), 493 (N2), 503 (N3), 513 (N4), 523 (N5), 533 (N6), 543 (N7), 553 (N8), and 623 K (N9). For this purpose 4 – 5 g of CZTS powder were loaded and sealed in an evacuated silica ampoule. Each ampoule was inserted into a muffle furnace and heated for 1 week. At the end of each run the silica ampoule was quenched in cold water in order to freeze the equilibrium state and hence the cations order at the annealing temperature. In addition, for the last sample (N10) a second annealing step at a temperature of 473 K for further two weeks was performed before second quenching.

2.2 Characterization

Investigations of the chemical composition were performed by electron microprobe analysis (EMPA) with a JEOL JXA 8200 SuperProbe equipped with 5 wavelength dispersive X-ray spectrometers (WDS) and an energy dispersive X-ray spectrometer (EDS). A calibration of the microprobe system was done by using elemental standards Cu, Zn, Sn and the mineral chalcopyrite for S in order to achieve reliable compositional parameters. High accuracy of the chemical composition could be obtained by measuring 25 grains of the CZTS phase averaging over 15 point measurements within each grain. The measurements of the samples were performed after the final quenching step.

The products were structurally characterized by neutron powder diffraction after checking phase purity and crystallinity by X-ray powder methods. Diffraction data were collected at the Forschungs-Neutronenquelle Heinz-Maier-Leibnitz Zentrum (MLZ, Garching) using the high resolution powder diffractometer SPODI (Ge (551) λ = 154.818(2) pm) [19]. For neutron experiments the samples were encapsulated in a vanadium container with 0.15 mm wall thickness and 9 – 10 mm inner diameter and

mounted in a sample changer. Structural refinements were performed by the Rietveld method [20] using the program FULLPROF Suite Version 2015 [21] by applying a Thompson-Cox-Hastings pseudo-Voigt function to describe the peak shape profile [22]. The kesterite type structure (space group $I\bar{4}$) was used as starting model for the refinements.

3 Results and discussion

In this work ten CZTS samples quenched from different temperatures in the region of 473 – 623 K were successfully synthesized. In order to ensure phase pure CZTS and to confirm the chemical composition of the synthesized samples the final powders were analyzed by WDS. This was done as also compositions beside the ideal stoichiometry can exhibit the kesterite structure. Studies on non-stoichiometric CZTS samples were carried out by Lafond et al. [23, 24] and extended by Valle-Rios et al. [25] leading to five off-stoichiometric CZTS types that can be described by different cation substitution reactions and formation of related point defect complexes. The results of our phase analyses show a homogenous composition for each sample, no secondary phases were found. The Cu/(Zn+Sn) and Zn/Sn ratios of the single phase CZTS samples were determined as 0.98 – 1.01 and 1.00 – 1.03 , respectively, thus by taking into account the experimental error of the microprobe system all samples can be considered as stoichiometric (see Figure 2).

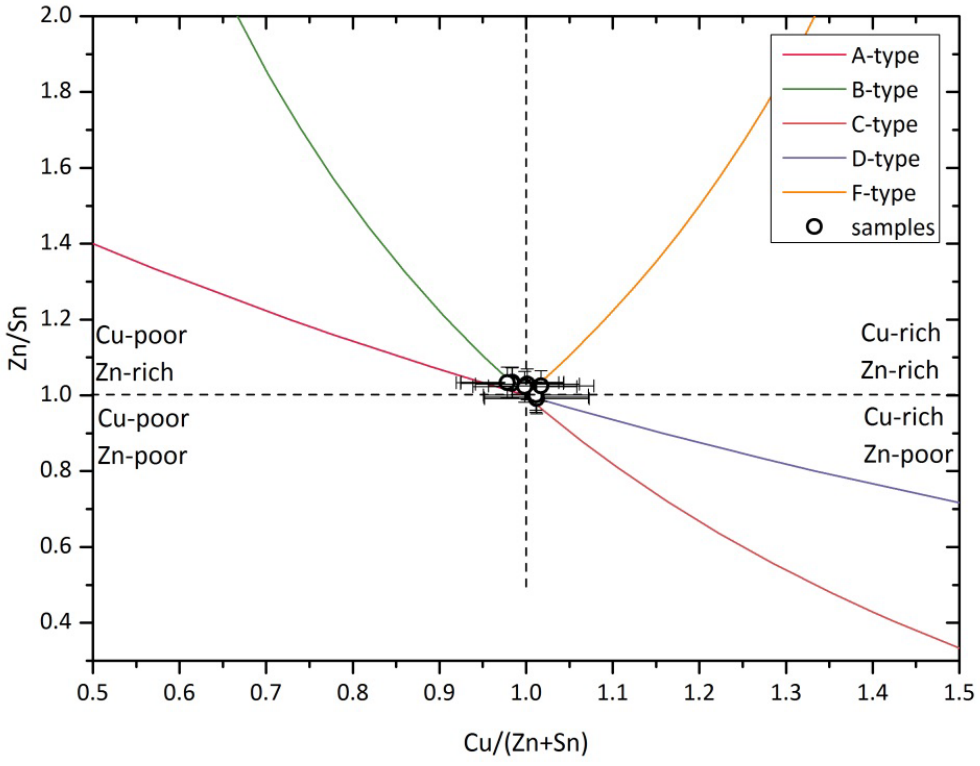

Figure 2 Cu/(Zn+Sn)-Zn/Sn plot showing the position of the ten prepared CZTS samples (lines – off stoichiometric types introduced by [23-25]).

The neutron powder diffraction patterns of all samples are depicted in Figure 3. All powders show high crystallinity. Looking at the diffraction patterns (see Figure 4) of samples N1, quenched from the lowest temperature (maximum order expected), and N9, quenched from the highest temperature (statistical distribution of Cu and Zn on sites 2c and 2d expected), it is clearly seen that the intensity of the superstructure reflection at 2θ = 18.3 ° is decreased for sample N9. This is a clear indication for a decreased order of the cations. However, no steady intensity decrease of the superstructure reflection as it is expected for increasing disorder is observed (see Figure 3). Hence, in order to track the order-disorder transformation in detail the crystal structure parameters of all nine samples were refined using the Rietveld method [21]. As the powders were all detected to be stoichiometric within the standard deviation the ideal composition Cu_2ZnSnS_4 was used for the structural refinements. The kesterite-type structure (space group $I\bar{4}$) was used as starting model for the refinements. Detailed cation distribution analyses were performed.

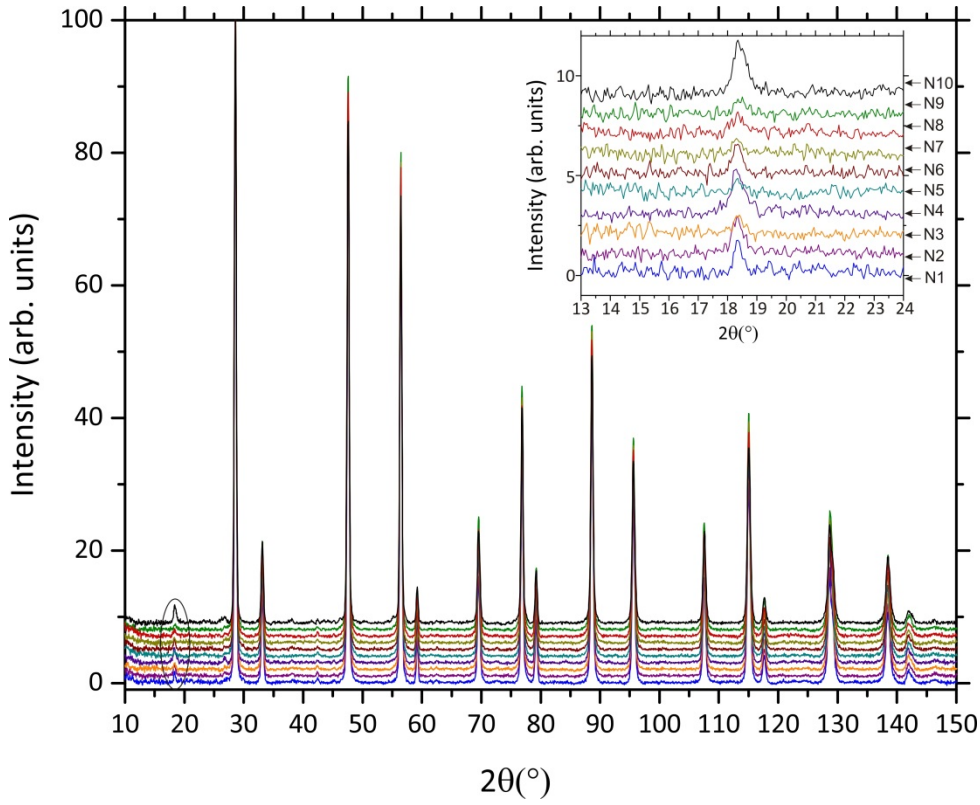

Figure 3 Neutron diffraction patterns of all synthesized samples measured at the high resolution powder diffractometer SPODI (λ = 154.818(2) pm). In the upper right corner an enlarged part of the superstructure reflection at 2θ = 18.3 ° is shown.

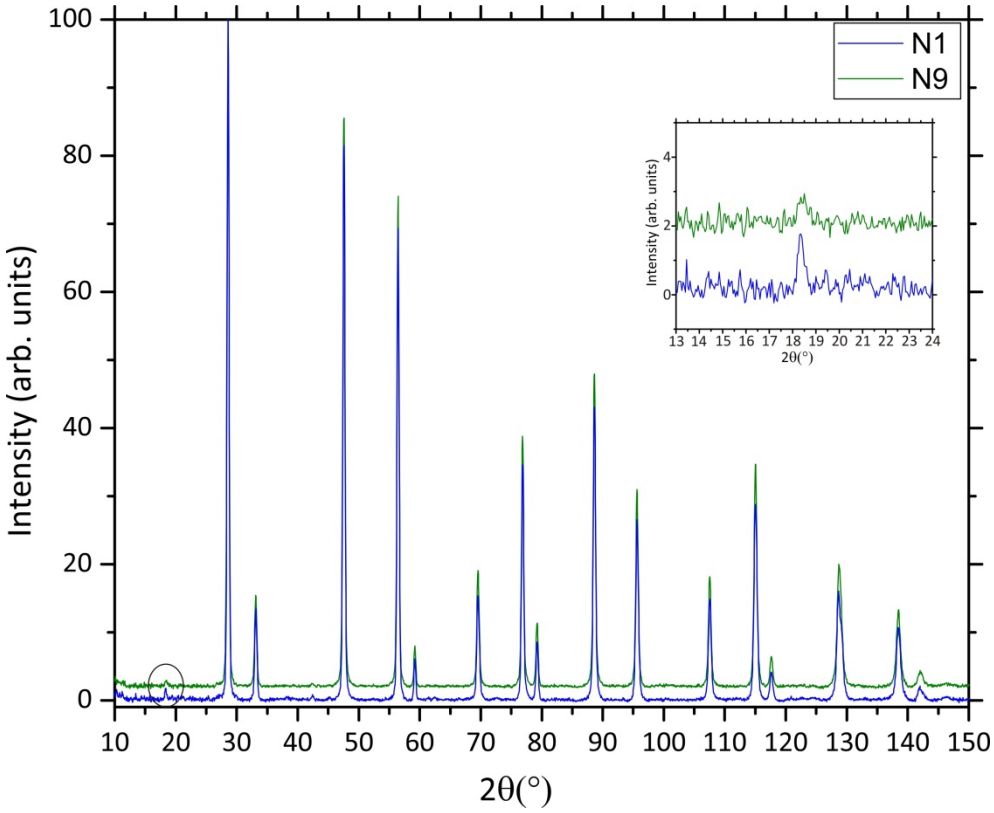

Figure 4 Comparison of the diffraction pattern N1 (473 K) and N9 (623 K). In the upper right corner an enlarged part of the reflection at 2θ = 18.3° is shown. Intensity of this superstructure reflection is decreasing which is a clear indication for a decreased order of the cations.

As a first approach the method of the average neutron scattering length was applied for determination of the cation distribution on the four positions. This method, which uses the refined site-occupancy values, was introduced by Schorr et al. [26].

As starting model the cations were distributed as follows: Cu on the Wyckoff positions 2a (0, 0, 0) and 2c (0, 1/2, 1/4), Zn on 2d (0, 1/2, 3/4), and Sn on 2b (0, 0, 1/2). These refined site occupancy value of position *i* (occ_i) is used to calculate the experimental average neutron scattering lengths $\bar{b}_i^{exp}$ according to Equation 1.

$$\bar{b}_i^{exp} = occ_i \cdot b_j \qquad \textbf{Eq. 1}$$

using the scattering lengths of the particular cation *j* on position *i* (b_{Cu} = 7.718 fm, b_{Zn} = 5.680 fm, b_{Sn} = 6.225 fm).

The obtained values of $\bar{b}_i^{exp}$ are compared with the neutron scattering lengths of Cu, Zn and Sn. An occurring deviation from the initial value and consequently a discrepancy of the occupancy value would predict that the cation site is not exclusively occupied by the presumed atom. In Figure 5 the refined cation site occupancy values occ_{2a}, occ_{2c}, occ_{2d} and occ_{2b} are depicted.

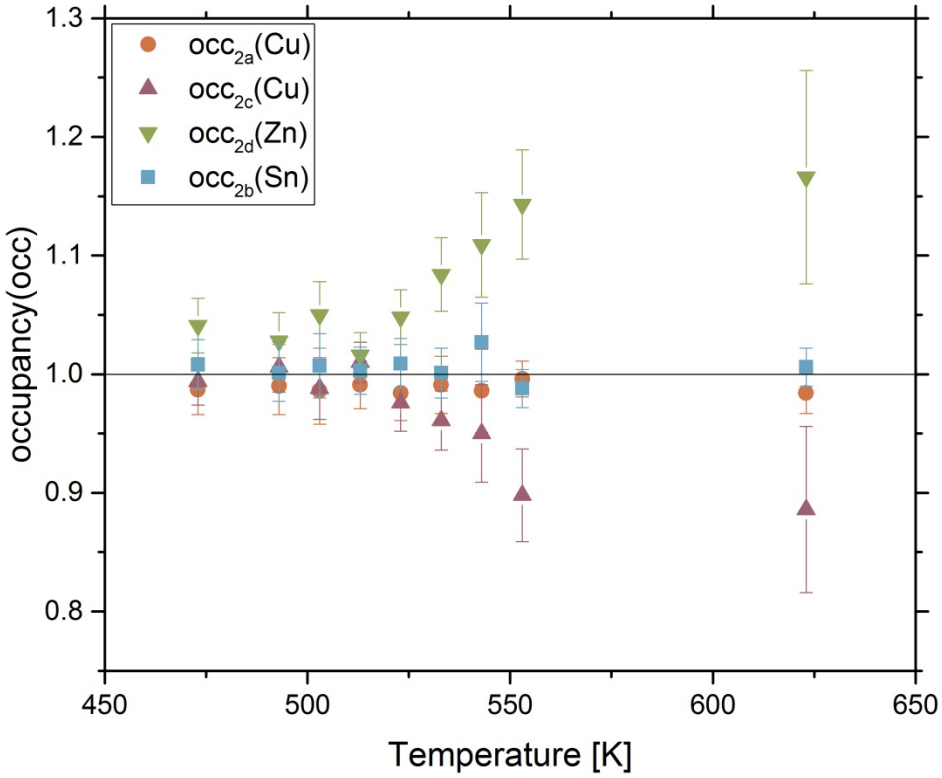

Figure 5 Temperature dependence of site occupancy values *occ_{2a}, occ_{2c}, $occ_{2d,}$ and occ_{2b}*. Cu fully occupies position 2a and Sn position 2b in the whole temperature range. Clear change visible at Cu_{2c} and Zn_{2d} – transformation from ordered to disordered kesterite

It is clearly seen that the occupancy values for Cu_{2a} and Sn_{2b} are not changing with increasing temperature. Within the standard deviation the nominal value of 1 is reached. From that we can predict that Cu fully occupies the 2a and Sn the 2b position within the whole temperature range. Looking at Zn and the remaining Cu on positions 2d and 2c, a clear change of the occupancy values is visible. While occ_{2c} is decreasing, occ_{2d} exceeds the value of 1 and a change from ordered to disordered kesterite can be presumed.

For the calculation of the cation distribution of Cu and Zn on positions 2c and 2d Equation 2 is used.

$$\bar{b}_i = x_i \cdot b_{Cu} + y_i \cdot b_{Zn} \qquad \textbf{Eq. 2}$$

where x_i and y_i are the fraction of Cu and Zn on the respective site. The results of these calculations are depicted in Figure 6.

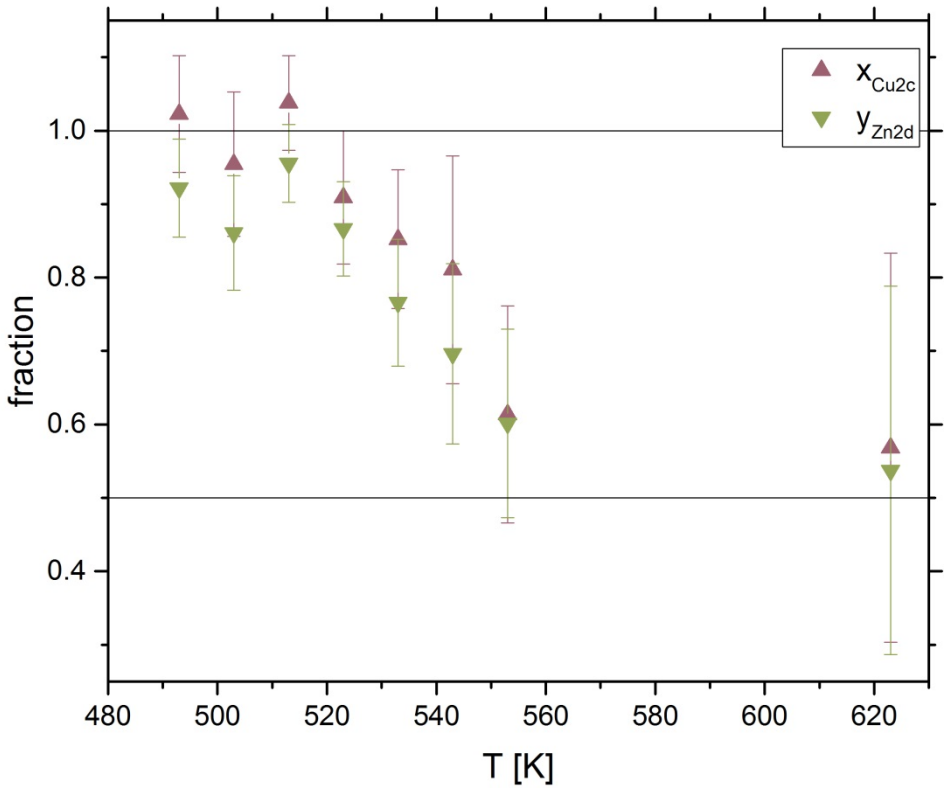

Figure 6 Temperature dependence of the fraction of Cu on cation site 2c and Zn and on the 2d site. A clear change from ordered to disordered kesterite is visible.

This figure shows that the values for site 2c and 2d differ from each other but lie in the same range within the standard deviation. Due to two consecutive calculation steps the error obtained from the Rietveld refinement is summing up and the error bars are getting very large.

In order to achieve more reliable values for the ratio of Cu and Zn on the two cation positions 2c and 2d, and to obtain a single order parameter for each temperature, a second approach was used refining the crystal structure. As the two cations on the sites 2a (Cu) and 2b (Sn) do not reveal any significant disorder in the whole temperature range these values were set to 1 and not refined during the procedure. Additionally, two side conditions were set: the sum of Cu and Zn on positions 2c and 2d must be 1 and both positions have to be fully occupied. As examples, two refinements for samples N1 and N9 are depicted in Figure 7. It is obvious that the refinements for both samples succeeded very well. It can be stated that the quality of the refinements is very good in the whole temperature range (see supplementary file).

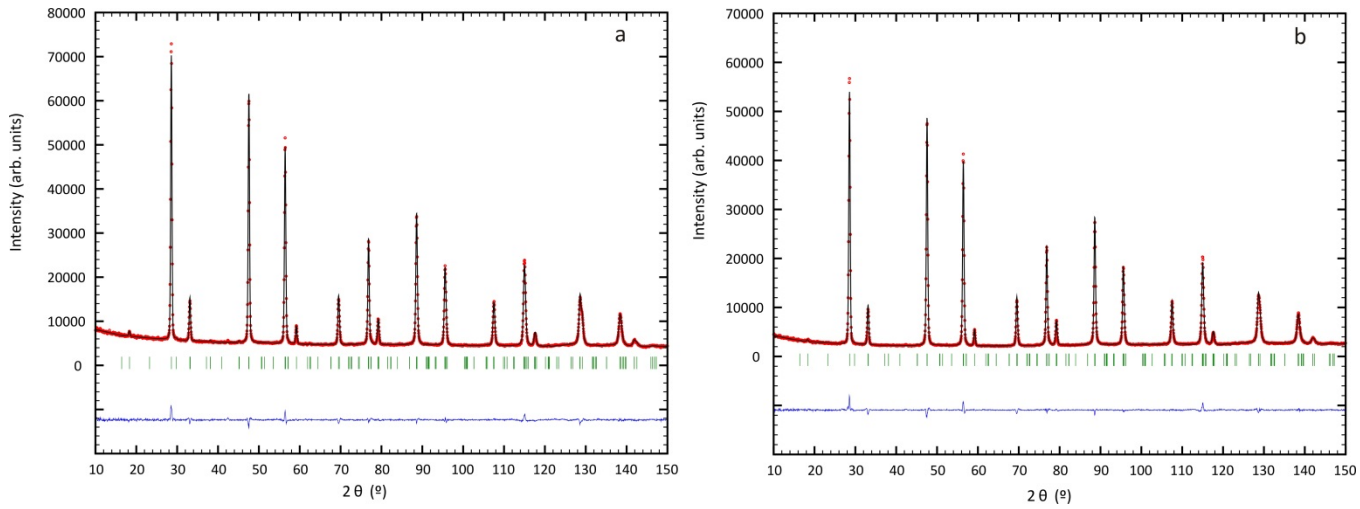

Figure 7 Selected neutron powder diffraction patterns of samples N1 (473 K) (a) and N9 (623 K) (b) with the results of the Rietveld refinements.

In order to discuss the ordering behavior within the frame of common phase transition theories an order parameter η, ranging from 0 (disorder) to 1 (complete order), was defined, related to the order-disorder process on the two cation positions 2c and 2d. η is related to the refined chemical order parameter s ($Cu(Cu_sZn_{1-s})_{Cu}(Zn_sCu_{1-s})_{Zn}SnS_4$; 1 = complete order, 0.5 = disorder) by η = 2s-1. The observed variation of η with temperature is depicted in Figure 8. Three different regions may be discerned:

I. Up to 513 K Cu and Zn are strongly ordered but no complete order within the standard deviation is reached.

II. Between 513 and 553 K there is a rapid decrease of order and the material is completely disordered at 553 K.

III. As expected, above 553 K complete disorder on 2c /2d positions in Cu_2ZnSnS_4 is reached. Cu and Zn show a statistical distribution on these sites. It should be mentioned that, in principle, the structural parameters of these samples (N8, N9) have to be refined in space group $I\bar{4}2m$, which is a minimal non-isomorphic supergroup of $I\bar{4}$ (index 2), as the positions 2c and 2d become equivalent and the symmetry of the structure increases. However, for better comparability of all samples and the determination of the order parameter these two samples were also refined in space group $I\bar{4}$. The refinements using space group $I\bar{4}2m$ are presented in the supplementary file. The agreement factors are as good as the same.

Common phase transition theories predict a critical power law (CPL) in the region below the critical temperature leading to the following equation for the temperature dependence of η:

$$\eta \propto \left(\frac{T_c - T}{T_c}\right)^{\beta} \qquad \textbf{Eq. 3}$$

with the critical temperature T_c and the critical exponent β. As may be anticipated from Figure 8, and known also from other compounds exhibiting an order-disorder transition [27], Equation 3 cannot be used for describing the whole low-temperature region. Nevertheless, a satisfactory fit is possible in region II (513 – 553 K).

The refined value of the critical exponent β is 0.57 ± 0.06 which is in agreement with a Landau-type behavior for a second order transition (β = 1/2). The critical temperature T_c for the transformation from ordered to disordered kesterite was determined as 552 ± 2 K. The fitted curve using Equation 3 is presented in Figure 8.

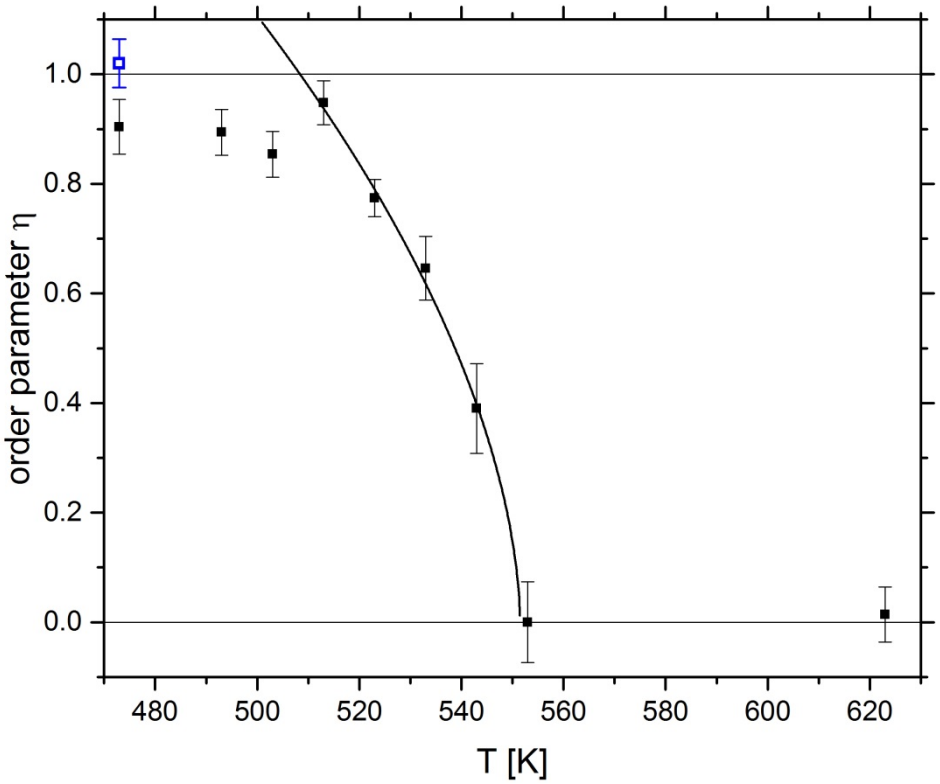

Figure 8 Temperature variation of the order parameter η and fit to Equation 3 (open symbol – sample N10). The order-disorder transformation follows a Landau type behavior for a second order transition.

It is remarkable that a fully ordered kesterite structure (η = 1 within the standard deviation) was not reached even at the lowest temperatures. Always a slight disorder is found in the samples. This is in agreement with the work of Scragg et al. [6] who claimed that a substantial concentration of disorder will always occur in practical samples. However, the highest value for the order parameter that was realized in his study on thin films was 0.8 for a sample annealed for 600 h (25 d) at 383 K. In our powder samples, a higher ordering could be achieved. The critical temperature determined by our neutron work differs slightly from the one determined by Scragg et al. [17] who published a value of T_c = 533 ± 10 K. Possible explanations of the difference may be their short annealing times of 1 hour to 24 hours of all their samples except the one described above (600 h) and their use of Zn-rich samples.

In order to investigate whether equilibrium is reached after an annealing time of 1 week, the sample N10, treated at 473 K, was additionally annealed for two weeks at the same temperature. The results of the Rietveld refinement are depicted in Figure 9 and Table 1. The refinements were carried out using both strategies described above, with similar results. Figure 10 (left) represents the experimental average neutron scattering length for the cation positions. The resulting cation distribution on the four sites 2a, 2b, 2c and 2d is depicted in Figure 10 (right). As shown in Table 1, this sample exhibits a full order (within the standard deviation) of Cu and Zn on their respective positions (for η, determined using refinement strategy 2, see Figure 8). Consequently, for Cu_2ZnSnS_4 very long annealing times are necessary to reach equilibrium at low temperatures. As a consequence, the above-discussed order parameters at low temperatures may slightly differ from the equilibrium values. This is also supported by the observation that the value at 513 K is larger compared to that of the samples treated at lower temperatures. Looking again at Figure 3, the behavior of the superstructure reflection at 2θ = 18.3° is easy to understand now. It clearly corresponds to the evolution of the order parameter.

Table 1 Refined structural parameters of sample N10

Neutron diffraction						
Structure type			kesterite			
Crystal system			tetragonal			
Space group			$I\bar{4}$ (No.82)			
Diffractometer			SPODI			
Wavelength			154.82 pm			
2θ range			1 – 150°			
a / pm			543.336(10)			
c / pm			1083.77(2)			
R_{Bragg} / %			2.40			
R_{wp} / %			2.80			
R_{exp} / %			1.68			
S			1.66			
Atom	**Wyckoff**	**x**	**y**	**z**	**B_{iso}**	**occ.**
Cu	2a	0	0	0	1.3(2)	1.00(3)
Cu	2c	0	1/2	1/4	1.8(3)	0.99(3)
Zn	2d	0	1/2	3/4	0.5(2)	1.01(3)
Sn	2b	0	0	1/2	0.3(2)	1.00(3)
S	8g	0.753(4)	0.7589(15)	0.8724(6)	0.728(14)	1

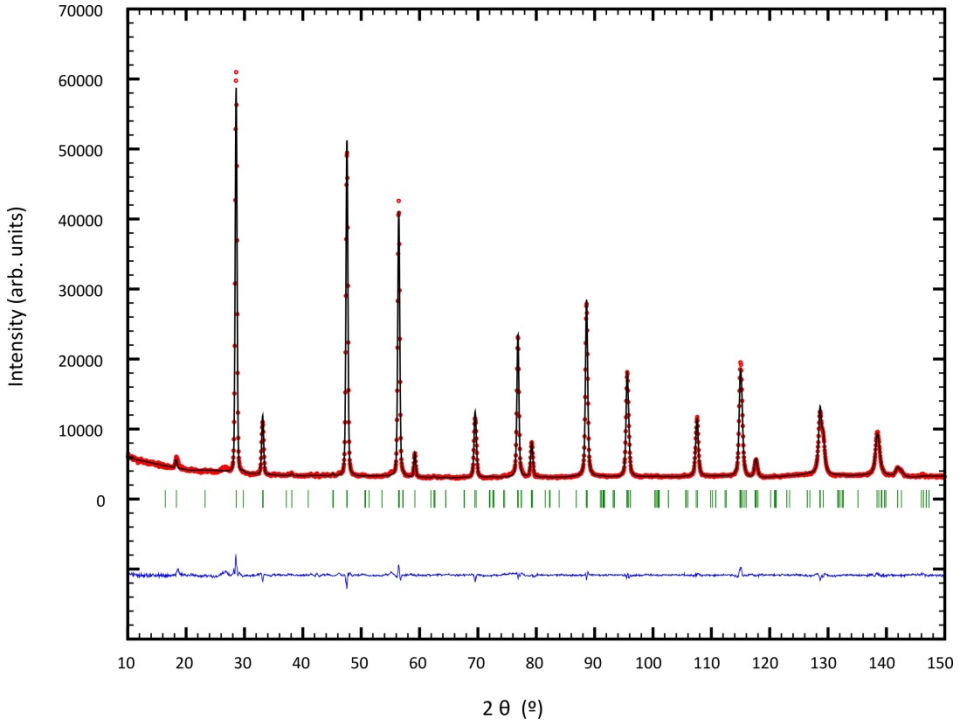

Figure 9 Neutron powder diffraction patterns of samples N10 (473 K) with the results of the Rietveld refinements.

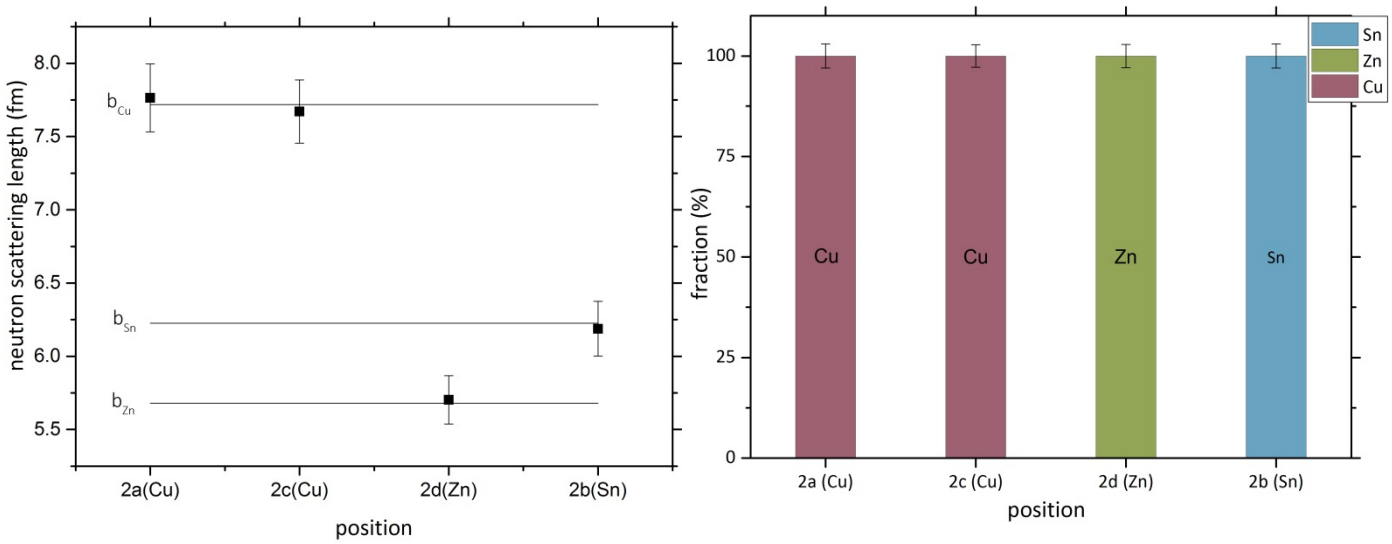

Figure 10 Experimental average neutron scattering length $\bar{b}_i^{exp}$ of the four cation sites of sample N10 (left) and resulting cation distribution (right). Within the standard deviation the sample exhibits a fully ordered kesterite structure.

4 Conclusions

In this study the order-disorder transition in Cu_2ZnSnS_4 was investigated using neutron diffraction techniques on samples annealed in the range of 473 – 623 K. A fully ordered (within the standard deviation) sample was prepared with an annealing time of three weeks at 473 K. As it is expected that the degree of order should severely influence the physical properties of Cu_2ZnSnS_4, these

investigations offer the possibility for directed preparation of materials with a defined order parameter which are an indispensable prerequisite for a deeper understanding of the correlations between crystal structure and electronic properties.

Acknowledgement

Financial support from the MatSEC graduate school of the Helmholtz Zentrum Berlin (HZB) in cooperation with the Dahlem Research School is gratefully acknowledged.

References

[1] S. Chen, X.G. Gong, A. Walsh, S.-H. Wei, *Appl. Phys. Lett.* 94 (2009) 041903/1-041903/3.
[2] J.J. Scragg, P.J. Dale, L.M. Peter, G. Zoppi, I. Forbes, *Phys. Status Solidi B* 245 (2008) 1772-1778.
[3] S. Siebentritt, S. Schorr, *Prog. Photovoltaics* 20 (2012) 512-519.
[4] W. Wang, M.T. Winkler, O. Gunawan, T. Gokmen, T.K. Todorov, Y. Zhu, D.B. Mitzi, *Adv. Energy Mater.* 4 (2014) 1301465/1-1301465/5.
[5] M. Grossberg, T. Raadik, J. Raudoja, J. Krustok, *Current Applied Physics* 14 (2014) 447-450.
[6] J.J.S. Scragg, J.K. Larsen, M. Kumar, C. Persson, J. Sendler, S. Siebentritt, C. Platzer Bjoerkman, *Phys. Status Solidi B* (2015) Ahead of Print.
[7] S. Schorr, *Sol. Energy Mater. Sol. Cells* 95 (2011) 1482-1488.
[8] L. Choubrac, M. Paris, A. Lafond, C. Guillot-Deudon, X. Rocquefelte, S. Jobic, *Phys. Chem. Chem. Phys.* 15 (2013) 10722-10725.
[9] S. Schorr, M. Tovar, *BENSC Experimental Report* (2006).
[10] A. Ritscher, J. Just, O. Dolotko, S. Schorr, M. Lerch, *J. Alloys Compd.* 670 (2016) 289-296.
[11] S. Schorr, H.-J. Hoebler, M. Tovar, *Eur. J. Mineral.* 19 (2007) 65-73.
[12] M.Y. Valakh, V.M. Dzhagan, I.S. Babichuk, X. Fontane, A. Perez-Rodriquez, S. Schorr, *JETP Lett.* 98 (2013) 255-258.
[13] A. Nagoya, R. Asahi, R. Wahl, G. Kresse, *Phys. Rev. B Condens. Matter Mater. Phys.* 81 (2010) 113202/1-113202/4.
[14] S. Chen, J.-H. Yang, X.G. Gong, A. Walsh, S.-H. Wei, *Phys. Rev. B: Condens. Matter Mater. Phys.* 81 (2010) 245204/1-245204/10.
[15] M. Paris, L. Choubrac, A. Lafond, C. Guillot-Deudon, S. Jobic, *Inorg. Chem.* 53 (2014) 8646-8653.
[16] A. Lafond, L. Choubrac, C. Guillot-Deudon, P. Fertey, M. Evain, S. Jobic, *Acta Crystallogr., Sect. B: Struct. Sci., Cryst. Eng. Mater.* 70 (2014) 390-394.
[17] J.J.S. Scragg, L. Choubrac, A. Lafond, T. Ericson, C. Platzer-Bjoerkman, *Appl. Phys. Lett.* 104 (2014) 041911/1-041911/4.
[18] S. Schorr, G. Gonzalez-Aviles, *Phys. Status Solidi A* 206 (2009) 1054-1058.
[19] M. Hoelzel, A. Senyshyn, N. Juenke, H. Boysen, W. Schmahl, H. Fuess, *Nucl. Instrum. Methods Phys. Res., Sect. A* 667 (2012) 32-37.
[20] H.M. Rietveld, *J. Appl. Crystallogr.* 2 (1969) 65-71.
[21] J. Rodriguez-Carvajal, *Abstracts of the Satellite Meeting on Powder Diffraction of the XV.Congress of the IUCr* (1990) 127.
[22] P. Thompson, D.E. Cox, J.B. Hastings, *J. Appl. Crystallogr.* 20 (1987) 79-83.
[23] A. Lafond, L. Choubrac, C. Guillot-Deudon, P. Deniard, S. Jobic, *Z. Anorg. Allg. Chem.* 638 (2012) 2571-2577.
[24] L. Choubrac, A. Lafond, C. Guillot-Deudon, Y. Moelo, S. Jobic, *Inorg. Chem.* 51 (2012) 3346-3348.
[25] L.E. Valle Rios, K. Neldner, G. Gurieva, S. Schorr, *J. Alloys Compd.* 657 (2016) 408-413.
[26] S. Schorr, C. Stephan, T. Toerndahl, R. Mainz, Wiley-VCH Verlag GmbH & Co. KGaA, 2011, pp. 347-363.
[27] H. Boysen, F. Frey, M. Lerch, T. Vogt, *Z. Kristallogr.* 210 (1995) 328-37.